SURFACE WATER-ICE DEPOSITS IN THE NORTHERN SHADOWED REGIONS OF CERES. T. Platz[1], A. Nathues[1], N. Schorghofer[2], F. Preusker[3], E. Mazarico[4], S.E. Schröder[3], S. Byrne[5], T. Kneissl[6], N. Schmedemann[6], J.-P. Combe[7], M. Schäfer[1], G.S. Thangjam[1], M. Hoffmann[1], P. Gutierrez-Marques[1], M.E. Landis[5], W. Dietrich[1], J. Ripken[1], K.-D. Matz[3], and C.T. Russell[8], [1]Max Planck Institute for Solar System Research, Justus-von-Liebig-Weg 3, 37077 Göttingen, Germany (platz@mps.mpg.de), [2]Univ of Hawai'i at Manoa, Honululu, USA, [3]DLR, Berlin, Germany, [4]GSFD, Greenbelt, USA, [5]Univ of Arizona, Tucson, USA, [6]Freie Universität Berlin, Berlin, Germany, [7]Bear Fight Institute, Winthrop, USA, [8]UCLA, Los Angeles, USA.

Introduction: Ceres, the largest object in the main asteroid belt, has a low bulk density of 2,162 kgm^{-3} [1] suggesting large quantities of water (liquid and/or solid) being present within the outer layer and mantle as models predicted [2-4]. Portions of water-ice prevalent in the upper surface sublimates and a fraction of this water can potentially be coldtrapped in polar shadowed regions [5-7]. Because Ceres has a low axis tilt of 4.028° [8], depressions and crater interiors may persist in permanent shadow. This study presents results of the first image-based analysis of permanently shadowed regions (PSRs) and reports the discovery of water-ice deposits within some of them [8].

Methods: The Framing Camera (FC; [9]) on the Dawn spacecraft imaged the northern polar region close to northern summer solstice, where shadows are at a minimum. For image analysis we used images from Survey Orbit (~410 m/px) and High-Altitude Mapping Orbit (HAMO; ~140 m/px). We define permanent shadows for those sites where the disk of the Sun never crosses the horizon (i.e., umbra). In radiance profiles, umbra is typically marked by a plateau. To determine at which radiance value umbra occurs, we developed a new approach by defining the threshold value near the north pole close to the terminator. This threshold value is then corrected for increasing solar radiation as a function of decreasing geographical latitude and longitudinal variations across a single image (i.e., varying local times). This correction also accounts for Ceres' oblateness (best-fit triaxial ellipsoid is 482×482×446 km). For Survey data only panchromatic images (filter F1) taken just before solstice were used whereas for HAMO data, F1 and colour data (F2, F3, F6, and F8) were utilised. Hence, for each filter individual threshold values at the same location were defined. Images from each orbit were stacked using improved spacecraft positioning and camera pointing kernels, binarised (white=1= sun lit; black=0=umbra), and averaged. Those pixels with nought values in the binarised average mosaic mark the locations where no direct sun light was received. However, to check that each site was imaged at many local times, the maximum latitude where full local time coverage is given had to be evaluated for both Survey and HAMO datasets. Survey data show complete time coverage between 65-90°N, whereas for HAMO data local time coverage is complete to only within 7° of the pole (i.e., 83°N) (Fig. 1).

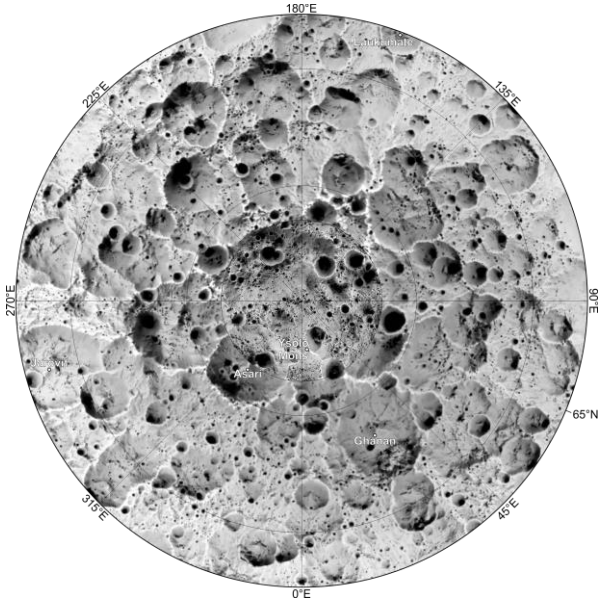

Fig. 1: Combined binary-averaged Survey and HAMO map for the region north of 65°N. Black areas represent permanent shadowed regions [8].

PSR craters and area size: The total estimated PSR area size (combined Survey and HAMO data) is 2,129±176 (1σ) km^2 or 0.15% of the northern hemisphere of Ceres. At least 634 craters (diameter range 0.5-74 km) host PSRs; 338 craters were mapped poleward of 83°N (Fig. 2). We conducted surveys on Low-Altitude Mapping Orbit (LAMO; ~35 m/px) and HAMO images to search for water-ice deposits as predicted by [7]. In 10 craters we found bright deposits in multiscattered light (Fig. 3). These deposits are located at lower pole-facing crater walls or off-centre on crater floors. At one location (crater #2) the bright deposit is briefly illuminated near summer solstice; here two VIR observations confirm the presence of diagnostic water absorption bands at 1.28 µm, 1.65 µm, and 2.0 µm (Fig. 4). The bright deposit has an absolute reflectance

of 0.10-0.16, higher in reflectance than those deposits found in Oxo Crater [10,11].

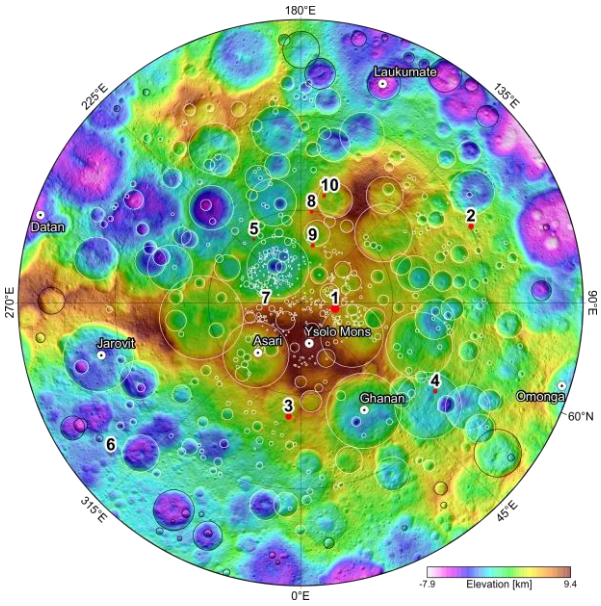

Fig. 2: Craters hosting PSRs. Labels 1-10 refer to craters hosting bright deposits. The map shows the region north of 60°N; black circles show craters potentially hosting PSRs [8].

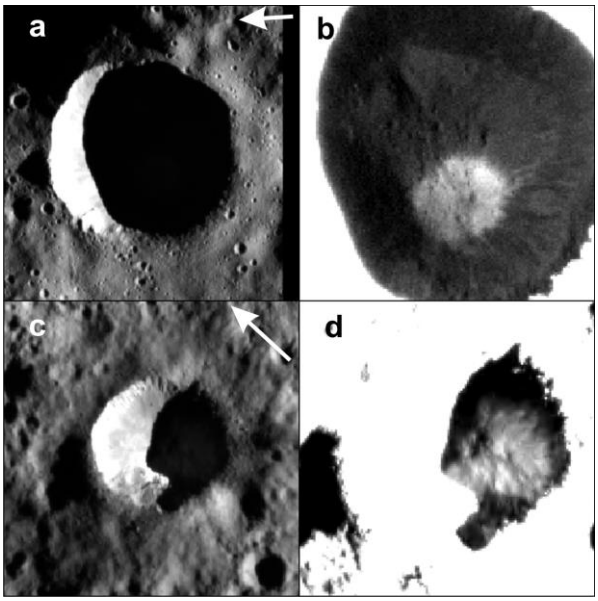

Fig. 3: Bright deposits in permanent shadow. (a-b) 6.6 km diameter crater located at 86.2°N/80.0°E. (c-d) 3.8 km diameter crater (#2) located at 69.9°N/114.0°E. Arrows point to north [8].

Discussion: Cold traps are characterised by H_2O loss rates of <1 $mGyr^{-1}$ corresponding to temperatures of 110K or less. Our detailed modelling of peak summertime temperatures within PSRs revealed 57K or less for a range of tested combinations (incidence angle, bowl-shaped vs. flat-floored craters, depth-to-diameter ratio). Ices such as H_2O, CO_2, NH_3, and SO_2 would be stable under these conditions.

Although the process of water molecule release through a variety of processes (e.g., sublimation of ice from shallow subsurface, discharge through cryovolcanic eruptions) and molecule transport on ballistic trajectories from low latitudes towards colder polar regions is somewhat understood, the lack of a more widespread distribution of bright deposits within PSRs is puzzeling. Ceres is a densely cratered body, in particular near the poles [12], hence, regolith mixing and gardening is likely a dominant process in disguising or destroying water-ice deposits. Alternatively, obliquity excursions with short-term periodicity [13] may prevent deposition of thick and widespread water-ice deposits in PSRs on Ceres. This is the subject of ongoing study [14].

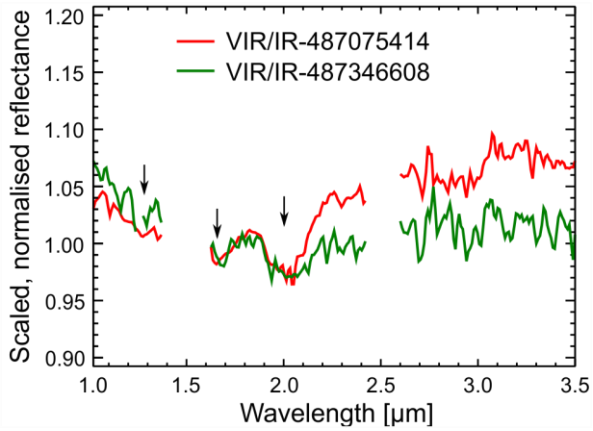

Fig. 4: Water-ice signatures in VIR spectra within crater #2. Water absorption bands are marked by arrows [8].

References: [1] Park R.S. et al. (2016) *Nature*, 537, 515-517. [2] Thomas P. et al. (2005) *Nature*, 437, 224-226. [3] Zolotov, M. Y. (2009) *Icarus*, 204, 183-193. [4] Castillo-Rogez J. C. and McCord T. B. (2010) *Icarus*, 205, 443-459. [5] Arnold J. R. (1979) *J. Geophys. Res.*, 84, 5659-5668. [6] Hayne P. O. and Aharonson O. (2015) *J. Geophys. Res.*, 120, 1567-1584. [7] Schorghofer N. et al. (2016) *Geophys. Res. Lett.*, 43, 6783-6789. [8] Platz T. et al. (2016) *Nature Astron.*, 1, 0007. [9] Sierks H. et al. (2011) *Space Sci. Rev.*, 163, 263-327. [10] Nathues A. et al. (2015) *Nature*, 528, 237-240. [11] Combe J.-Ph. et al. (2016) *Science*, 353, 3010. [12] Hiesinger H. et al. (2016) *Science*, 353, 4759. [13] Bills B.G. and Scott B.R. (2017) *Icarus*, 284, 59-79. [14] Ermakov A. et al. (2016) *AGU Fall Meeting*, P43C-2126.